Brain segmentation in magnetic resonance human head scans using multi-seeded region growing

K. Somasundaram and P. Kalavathi*

This paper presents a skull stripping method to segment the brain from MRI human head scans using multi-seeded region growing technique. The proposed method has two stages. In Stage-1, the brain in the middle slice is segmented, the brains in the remaining slices are segmented in Stage-2. In each stage, the proposed method is required to identify the rough brain mask. The fine brain region in the rough brain mask is segmented using multi-seeded region growing approach. The proposed method uses multiple seed points which are selected automatically based on the intensity profile of grey matter (GM), white matter (WM) and cerebrospinal fluid (CSF) of the brain image. The proposed brain segmentation method using multi-seeded region growing (BSMRG) was validated using 100 volumes of T1, T2 and PD-weighted MR brain images obtained from Internet Brain Segmentation Repository (IBSR), LONI and Whole Brain Atlas (WBA). The best Dice (D) value of 0·971 and Jaccard (J) value of 0·944 were recorded by the proposed BSMRG method on IBSR dataset. For LONI dataset, the best values of D=0·979 and J=0·960 were obtained for the sagittal oriented images by the proposed method. The performance consistency of the proposed method was tested on the brain images of all types and orientation and have and produced better and stable results than the existing methods Brain Extraction Tool (BET), Brain Surface Extraction (BSE), Watershed Algorithm (WAT), Hybrid Watershed Algorithm (HWA) and Skull Stripping using Graph Cuts (GCUT).

Keywords: Brain segmentation, Skull stripping, Multi-seeded region growing, Brain extraction method, MRI brain image

Introduction

Among the various medical imaging techniques, MRI is one of the most widely used imaging techniques in the medical field. It is a non-invasive, non-destructive, flexible imaging tool.[1] MRI is particularly suitable for brain studies, because it can image both interior and exterior brain structures with a high degree of anatomical details using which even the minute changes in these structures that occur over time period can be detected.

Several techniques have been developed for MR brain image segmentation and there is no standardised generic technique that can produce satisfactory results for all types of brain images. Moreover, the presence of non-brain tissues is considered as the major challenge for brain image segmentation techniques. Therefore, most of the brain image analysis techniques such as registration, tissue classification or compression[2] need to eliminate these non-brain tissues as a pre-processing step commonly referred to as skull stripping. A number of automated and semi-automated brain segmentation algorithms available in the literature.[3–19] Among all these methods, Brain Extraction Tool (BET),[5] Brain Surface Extraction (BSE),[6] Watershed Algorithm (WAT),[7] Hybrid Watershed Algorithm (HWA)[8] and Skull Stripping using Graph Cuts (GCUT)[9] are the popular methods. Further, Park and Lee[12] developed a skull stripping method for T1-weighted MR brain images based on 2D region growing method. It aims to automatically detect two seed regions of the brain and non-brain by using a mask produced by morphological operations. Then, the seed regions were expanded using 2D region growing algorithm, based on the general brain anatomical information.

Each of these existing methods has their own merits and demerits.[4] Most of the existing automated skulls stripping algorithms are applicable only to T1-weighted MR human brain images and do not work well on all the three orientations namely axial, sagittal and coronal (WAT, HWA and GCUT methods). Moreover, the complexity in human brain anatomy, variation in shape and size of the brain, use of different pulse sequences during MR imaging process, overlapping signal intensities in brain images, varying contrast properties between the brain tissues, poor registration of brain image, weak boundaries between brain and non-brain tissues and the

Department of Computer Science and Applications, Gandhigram Rural Institute, Deemed University, Gandhigram, Tamil Nadu 624 302, India

*Corresponding author, email pkalavathi.gri@gmail.com

Received 23 May 2013; accepted 1 November 2013
DOI 10.1179/1743131X13Y.0000000068

presence of various imaging artifacts[20] are the posing challenges to the development of efficient and automatic skull stripping method.

In this paper, an automatic brain segmentation method using multi-seeded region growing (BSMRG) is proposed to segment the brain from T1, T2 and PD-weighted MRI human head scans in all the three orientations. Experimental results using the proposed method on 100 volumes of T1, T2 and PD-weighted images obtained from Internet Brain Segmentation Repository (IBSR),[21] LONI Probabilistic Brain Atlas (LPBA40)[22] and Whole Brain Atlas (WBA)[23] show that the proposed method gives better results than that of the five existing skull stripping methods BET, BSE, WAT, HWA and GCUT.

The remaining part of the paper is organised as follows. In the section on 'Methods and materials', the proposed BSMRG method and the details about the brain image datasets used to evaluate the proposed method are described. The results and discussion are given in the section on 'Results and discussion' and the conclusion is given in the section on 'Conclusion'.

Methods and materials

The proposed BSMRG method is a two-stage brain segmentation method. The brain in the middle slice of a volume is segmented in Stage-1 and the brains in the remaining slices are segmented in Stage-2. Both Stage-1 and Stage-2 of this method consists of operations such as brain image preprocessing, rough brain image extraction, seed points selection and fine brain segmentation using multi-seeded region growing method. The overall flowchart of the proposed brain segmentation method is given in Fig. 1.

Stage-1: brain segmentation from middle slices

First, the middle slice of a brain volume is taken as the input image and it is preprocessed to enhance its contrast to obtain the binary image. Since the binary image are easier to process and analyse than the grey level images, the brain segmentation method BSMRG presented in this paper is required to produce a binary form of the original brain image in the first step. The binary image reduces the complexity in the image data and simplifies the brain image segmentation process. However, the luminance non-linearity introduced by MR imaging device produce a low/high-contrast bias in the brain image and this variations in the image contrast often influence the output of image binarisation. Therefore, in this proposed method the input brain image is preprocessed using the contrast enhancement technique[22] and image binarisation method.[23]

The binary form of the brain image g may contain several holes. Although the holes in the binary image may help to separate the weakly connected substructures, the presence of small holes produces undesirable results during morphological erosion process. Therefore, the small holes are to be filled before applying the erosion operation. It is achieved using the morphological reconstruction operation[26] and the hole filled binary image is denoted by g_{HF}. The complement of both small and large holes in g_{HF} are identified by performing logical AND operation as given in equation (1).

$$\overline{H}_{\mathrm{SL}} = g_{\mathrm{HF}} \wedge \overline{g} \tag{1}$$

where $\overline{g}$ is the complement of image g, $\wedge$ denotes the AND operation and $\overline{H}_{\mathrm{SL}}$ is the complement of both small and large holes. The complements of holes which are larger than a specified size S are then removed to obtain $\overline{H}_{\mathrm{S}}$, which contains only the complement of small holes. Then, the image with the large holes denoted as g_{LH} is obtained as

$$g_{\mathrm{LH}} = \overline{H}_{\mathrm{S}} \vee g \tag{2}$$

where $\vee$ denotes the logical OR operation.

Then, the binary erosion is applied on g_{LH} using a structuring element (SE) of size O_3 (Fig. 2) to disconnect the weakly connected substructures around the image and the eroded image is denoted as g_{E}.

The brain in the middle slice is recognised as Largest Connected Component (LCC). Therefore, it is necessary to search for LCC in g_{E}, for which all the connected regions in g_{E} are labelled using run length encoding technique.[27] The aggregation of regions in g_{E} is expressed as

$$g_{\mathrm{E}} = \sum_{\mathrm{i}=1}^{\mathrm{n}} R(i) \tag{3}$$

where $R(i)$ is the ith isolated region. The area of ith region $R(i)$ is computed as $R_{\mathrm{A}}(i)$. The LCC in g_{E} denoted as g_{LCC} is selected as

$$g_{\mathrm{LCC}} = R\left(\underset{1 \le \mathrm{i} \le \mathrm{n}}{\arg \max} (R_{\mathrm{A}}(i)) \right) \tag{4}$$

In order to recover the brain pixels lost during the erosion operation, the selected g_{LCC} is dilated with O_3 to get the rough brain mask g_{RBM}.

The g_{RBM} may contain some large holes. The large holes present in g_{RBM} are filled with a hole filling procedure[26] and the resultant g_{RBM} is subjected to dilation by O_3. Since, in many cases, it is impractical to restore the original shape of the objects which are dilated with SEs of the same size or lesser.[9]

Using the rough brain mask g_{RBM}, the rough brain area is selected as

$$g_{\mathrm{RB}} = \begin{cases} f(x,y) & \text{if } g_{\mathrm{RBM}}(x,y) = 1 \\ 0 & \text{otherwise} \end{cases}. \tag{5}$$

After extracting the rough brain image g_{RB}, the seed points in g_{RB} are selected to begin the process of region growing segmentation. Selection of seed point is an important event in region growing methods, which directly influences the segmentation result. Usually, the seed points are to be selected inside of ROI, if it is selected outside of ROI then the final segmentation results would be definitely incorrect. In this method, due to varying tissue types and contrast properties of MR brain images, the multiple seed points are chosen within the brain region in order to get accurate segmentation result. The seed area for this purpose is identified by drawing a seed area circle inside the rough brain image g_{RB}. The radius of the seed area circle is computed by taking half of the average of the distance from the centre of g_{RB} towards the brain border in the four directions $(x, y, -x, -y)$ and is given as

$$r = \frac{1}{2}\left(\frac{\sum d_{\mathrm{i}}}{4} \right) \tag{6}$$

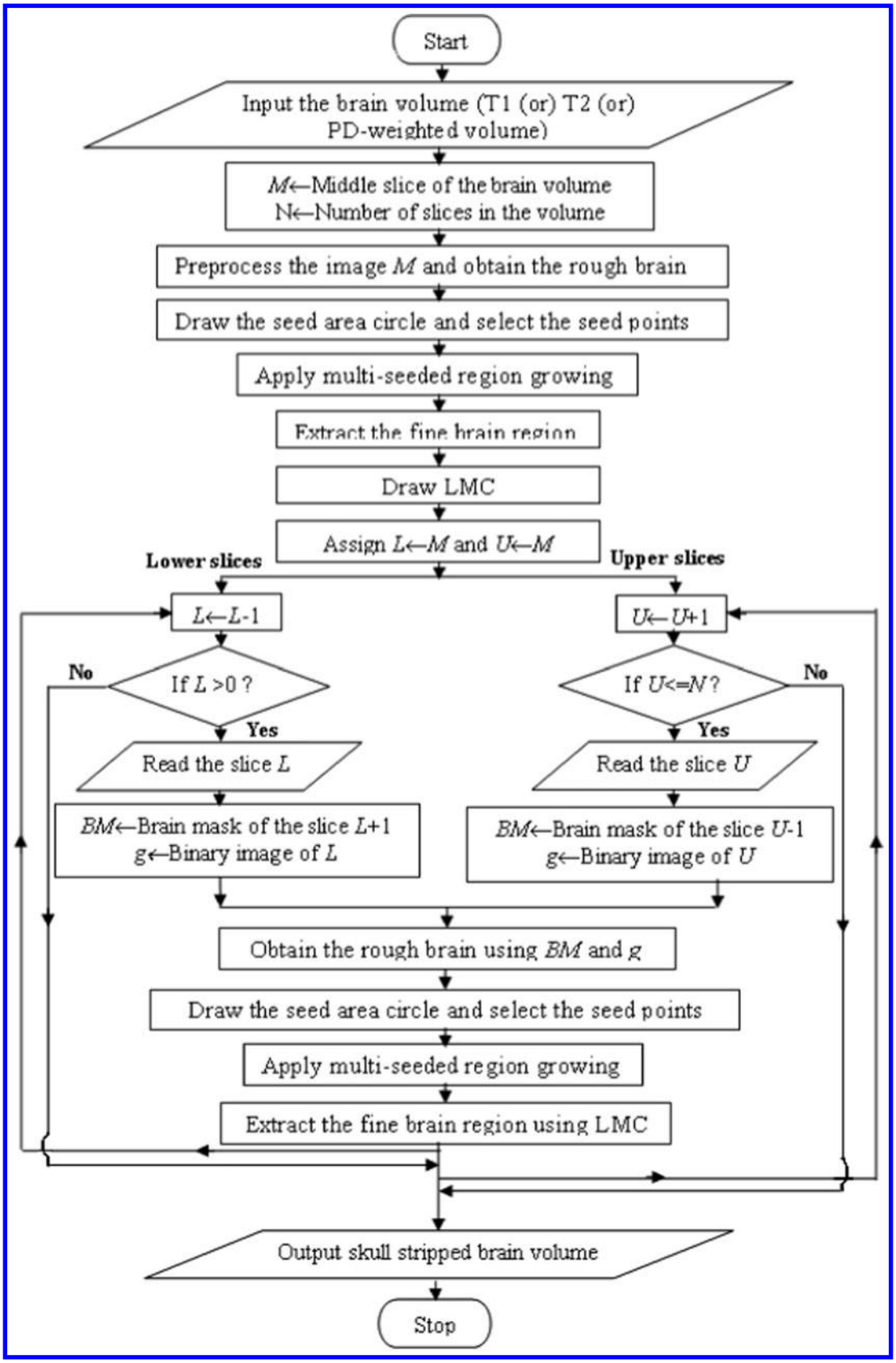

1 Overall flowchart of BSMRG method

where $i=1, 2, \ldots, 4$ represents the four directions and d_i represents the distance from the centre of the extracted brain to the border on right ($i=1$), top ($i=2$), left ($i=3$) and bottom ($i=4$). If the computed radius r is found to be larger than any d_i value, then it is reduced to minimum of d_i, so that the seed area circle never grows to the outside of the brain region. Among all the pixels in the seed area, only a subset of pixels are selected as the seed points. Because the experimental results show that selecting all the pixels in the seed area as seed points

0	0	1	1	1	0	0
0	1	1	1	1	1	0
1	1	1	1	1	1	1
1	1	1	1	1	1	1
1	1	1	1	1	1	1
0	1	1	1	1	1	0
0	0	1	1	1	0	0

2 Structuring element of size O_3

deviates the growing process and thus considerable number of non-brain tissues are included in the final segmentation. Therefore, it is essential to devise a mechanism to identify some set of pixels as seed points among the pixels in the selected seed area.

In this method, the seed points are selected automatically based on the intensity properties of grey matter (GM), white matter (WM) and cerebrospinal fluid (CSF) tissues of the selected seed area that lies within the brain region as illustrated in Fig. 3. The unique intensity values of these tissues in the seed area are considered for seed point selection. The set of distinct points in the seed list is denoted as SL and then the pixels in SL are categorised into three groups, namely, SL_{low}, SL_{middle} and SL_{high} using K-means clustering,[28] which may represent the group containing bright pixels values, grey pixels values and dark pixels values, respectively.

The bright, grey or dark pixel represents the different brain tissue contrast properties in T1-, T2- and PD-weighted images and their corresponding seed list group classifications are given in the Table 1. This table represents the probable seed list grouping of brain tissues CSF, GM and WM into SL_{low}, SL_{middle} and SL_{high} based on the contrast property of T1-, T2- and PD-weighted MR brain images. In this method T1-, T2- and PD-weighted images are treated separately to select the seed points. Since in the T1-weighted images, the CSF appears as dark pixels, GM as grey pixels and WM as bright pixels, the CSF, GM and WM of T1-weighted images may be grouped into SL_{high}, SL_{middle} and SL_{low} lists, respectively. In T2-weighted images, CSF is represented as bright pixel, GM and WM are represented as grey pixels and so they may be included in SL_{low} and SL_{middle} lists, respectively. Similarly, in PD-weighted images, CSF appears as grey pixels and GM as bright pixels, since they may be placed into SL_{middle} and SL_{high} lists, whereas the WM of PD-weighted image appears as isointense, and thus, they may be grouped into either SL_{low} or SL_{middle} list depending on their intensity levels.

Then the pixels in the SL_{middle} list are selected as seed points. If SL_{high} or SL_{low} is chosen as a seed point, then at the worst case, instead of segmenting the whole brain, it will segment only the CSF tissues in T1-weighted or CSF tissue in T2-weighted brain image, respectively. Therefore, in the proposed approach, the pixels in the SL_{middle} list are selected as seed points. Then, the region growing algorithm is applied by taking all the seed points in SL_{middle} to obtain the fine brain mask. The region is iteratively grown by comparing all the unallocated neighbouring pixels to the region. The difference between a pixel's intensity value and the region's mean is used as a measure of similarity. The pixels with the smallest difference measured this way are allocated to the respective regions. This process stops when the intensity difference between region mean and new pixel become larger than the threshold (t) (i.e. similarity measure). The procedure of multi-seeded region growing approach is given in Algorithm 1.

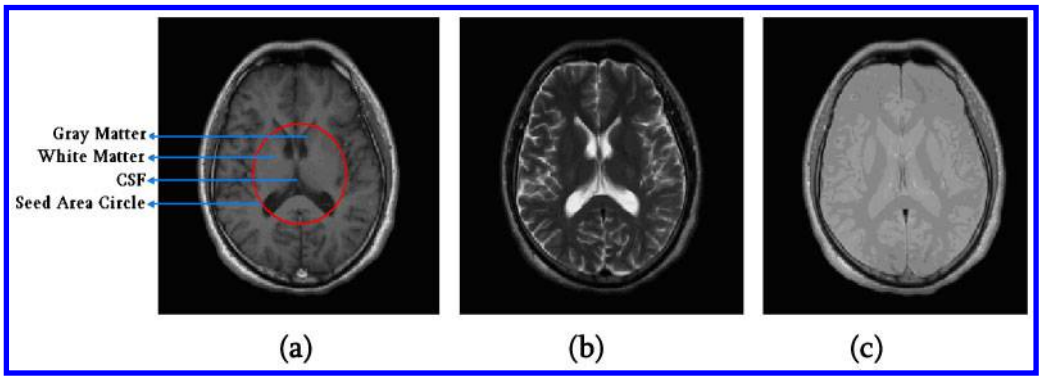

3 Brain tissue contrast in MR brain images: *a* T1-weighted image; *b* T2-weighted image; *c* PD-weighted image

Table 1 Seed list group classification of CSF, GM and WM tissues on T1-, T2- and PD-weighted brain images

	Brain tissue		
Image type	Cerebrospinal fluid (CSF)	Grey matter (GM)	White matter (WM)
T1	SL_{high}	SL_{middle}	SL_{low}
T2	SL_{low}	SL_{middle}	SL_{middle}
PD	SL_{middle}	SL_{low}	SL_{low} or SL_{middle}

Algorithm 1: Multi-Seeded Region Growing (MRG)

Input: 2D array representing the intensity of the input image and a set of seed points S.
Output: Skull-stripped brain image.
1. Create the region R to hold the pixels.
2. For each seed point 's' in S, do the Steps (3)–(5).
3. Add the seed point 's' into R if it is not already in R.
4. Consider the new neighbour k of 's'.
   i. Compute the mean μ of the region R.
   ii. Start the region growing procedure to add the neighbouring pixels into the region R when the intensity difference between the region R and possible new neighbour k is less than or equal to the threshold t, i.e. $|\mu - k| \leq t$.
   iii. Repeat Step (4) until no more neighbouring pixels are added to the region R.
5. Remove the seed point 's' in S and repeat Step (2).

After segmenting the fine brain, a landmark circle (LMC) is defined on the segmented middle brain to correctly extract the brain in the remaining slices. However, some of the existing skull stripping methods such as BSE have failed to extract the brain in the lower and upper slices of the brain volume, where the brain appears in more than one connected regions. This problem is solved by fixing an imaginary cylinder at the cenrte of the middle slice of the brain volume and is likely to pass through all the brain regions in the remaining lower and upper slices, irrespective of whether the brain is composed of one or more connected components. For this purpose, the LMC is defined similar to drawing of seed area circle which is used for selecting the brain regions in the remaining slices of that volume in Stage-2. The process involved in Stage-1 of BSMRG method is illustrated in Fig. 4.

Stage-2: brain segmentation in the remaining slices

The process of segmenting the brain regions in the remaining slices of the input brain volume is described in this stage. The gamma corrected input brain image of the remaining slices is converted into binary form using the methods given in Refs. 24 and 25. Then, using the previous adjacent brain mask BM, the rough brain mask is generated. To obtain the rough brain mask g_{RBM}, each connected regions in the input brain image g is labelled with numbers 1, 2, 3 and so on. Then the labelled regions which are overlapping with the previous brain mask BM are combined to produce the rough brain mask g_{RBM}.

Then the Percentage of Overlap (PO) is computed between the current g_{RBM} and BM by equation (7).

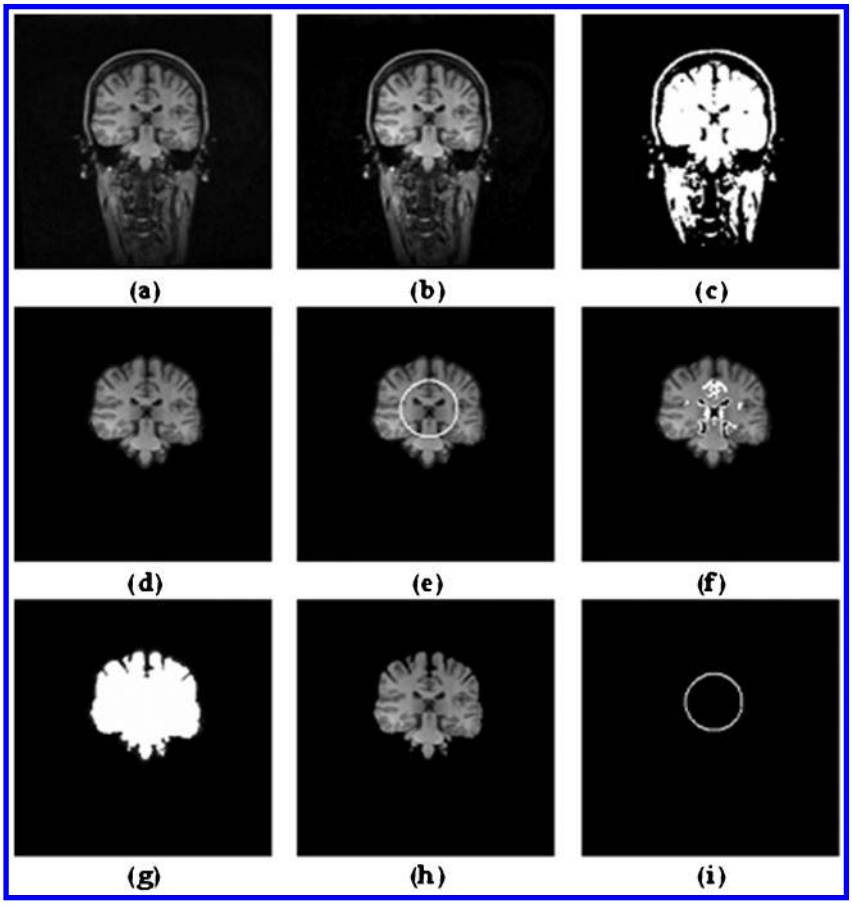

4 Brain extraction in middle slice by BSMRG method: *a* original image; *b* contrast enhanced image; *c* binary image; *d* selected rough brain; *e* identified seed area on the rough brain (white circle); *f* selected seed points (white pixels); *g* result of region growing; *h* segmented fine brain region; *i* defined LMC

$$PO(g_{\mathrm{RBM}},BM)=\frac{T(g_{\mathrm{RBM}}\cap BM)}{T(g_{\mathrm{RBM}})}\times 100 \quad (7)$$

Higher percentage of PO denotes that the g_{RBM} is similar in shape to that of the previous adjacent brain mask and is not connected with non-brain regions. If weak edges exist in the brain slices, the rough mask g_{RBM} may contain many connected non-brain regions producing lower PO value. These connected non-brain regions are separated by applying morphological erosion operation by using SE of size O_3. Sometimes, the erosion operation fails to separate the connected regions due to the strong existence of weak edges between the brain and non-brain tissues, those slices can be identified by calculating PO value. For such slice, the same pervious brain mask BM is used as g_{RBM} and is obtained as given in equation (8).

$$g_{\mathrm{RBM}}(x,y)=\begin{cases}1 & \text{if } BM(x,y)=1\\ 0 & \text{otherwise}\end{cases}. \quad (8)$$

Then the rough brain mask g_{RBM} is dilated by O_3 to recover brain pixels lost during erosion operation or if g_{RBM} is obtained using the previous brain mask BM, predicting that the current rough brain mask may sometimes be slightly larger than the previous brain mask.

After extracting the rough brain mask, the rough brain image g_{RB} is obtained using equation (5). The seed area and the seed points in g_{RB} are selected as given in Stage-1. Then the fine brain is segmented using the multi-seeded region growing method by Algorithm 1.

Sometimes, it is difficult to select the brain region in the remaining slices when the brain appears in many regions. Usually, the brain in the top and bottom slice of the brain volume may contain more than one connected regions. Therefore, to accurately extract all the brain regions of a slice, the LMC circle defined in Stage-1 is used. A set of pixels which are not separated by a boundary are called as a connected region. These connected regions are separated by neighbourhood and region labelling process. The proposed methods uses four-connected neighbourhood to identify the connected components in a given image. After separating the connected regions, the brain regions in the fine brain image is selected by finding the regions, which are partially or fully overlap with the LMC and the rest are discarded.

Performance evaluation metrics

To evaluate the performance of the proposed method Jaccard similarity index (J), Dice coefficient (D), false positive rate (FPR) and false negative rate (FNR) are calculated. The Jaccard similarity index (J)[29] is given by:

$$J(S_1,S_2)=\frac{|S_1\cap S_2|}{|S_1\cup S_2|} \quad (9)$$

The Dice coefficient (D)[30] is given by:

$$D(S_1,S_2)=\frac{2|S_1\cap S_2|}{|S_1|+|S_2|} \quad (10)$$

where S_1 represents the total pixels of the image obtained by the proposed method and S_2 represents the total pixels in the image obtained from ground truth data (gold standard).

The segmentation errors[3] false positive rate (FPR) and false negative rate (FNR) are used to measure the misclassification done by the proposed segmentation method. FPR is the ratio of the number of pixels incorrectly classified as brain region to number of non-brain region and false positive pixels. FNR is the ratio of the number of pixels incorrectly classified as non-brain region to number of brain region and false negative pixels. The FPR represents the degree of under segmentation and the FNR represents the degree of over segmentation. The FPR and FNR are computed as:

$$FPR=\frac{|FP|}{|TN|+|FP|} \quad (11)$$

$$FNR=\frac{|FN|}{|TP|+|FN|} \quad (12)$$

where TP and FP are true positive and false positive, which are defined as the number of voxels correctly and incorrectly classified as brain tissue by the proposed method. TN and FN are true negative and false negative, which are defined as the number of voxels correctly and incorrectly classified as non-brain tissue by the proposed method.

Brain image datasets used

Dataset-1

Twenty volumes of T1-weighted images were obtained from IBSR.[21] It contains MR brain volumes obtained from young-middle aged normal individuals. Each volume consists of T1-weighted 2D sequential coronal slices with dimensions of 256×256 pixels. The number of slices ranges from 60 to 65 and the slice thickness is 3·1 mm.

Dataset-2

The second datasets contains 40 volumes of T1-weighted brain images obtained from LONI.[22] It consists of 40 normal coronal volumes and their corresponding manually skull stripped images of 20 male and 20 female subjects, ages varies from 19 to 40 years and the mean age is 29·2 years. The dimension and inter slice gap are $256\times256\times124$ and $0{\cdot}86\times0{\cdot}86\times1{\cdot}5$ mm^3 voxel^{-1} for 38 subjects, $256\times256\times120$ and $0{\cdot}78\times0{\cdot}78\times1{\cdot}5$ mm^3 voxel^{-1} for two subjects, respectively.

Dataset-3

Twenty volumes of normal and abnormal brain images were collected from WBA.[23] Each volume consists of T2-weighted axial slices with dimensions of 256×256 pixels. The slice thickness varies from 2 to 5 mm with 260 mm field of view. The number slices ranges from 18 to 56.

Dataset-4

This dataset contains 20 PD-weighted axial slices obtained from WBA.[23] It contains both normal and abnormal volumes with dimensions of 256×256 pixels, slice thickness varies from 2 to 5 mm, field of view is 260 mm and the number slices ranges from 17 to 55.

Results and discussion

The proposed BSMRG method is evaluated to assess its quantitative and qualitative performance using 100 volumes of T1-, T2- and PD-weighted images of

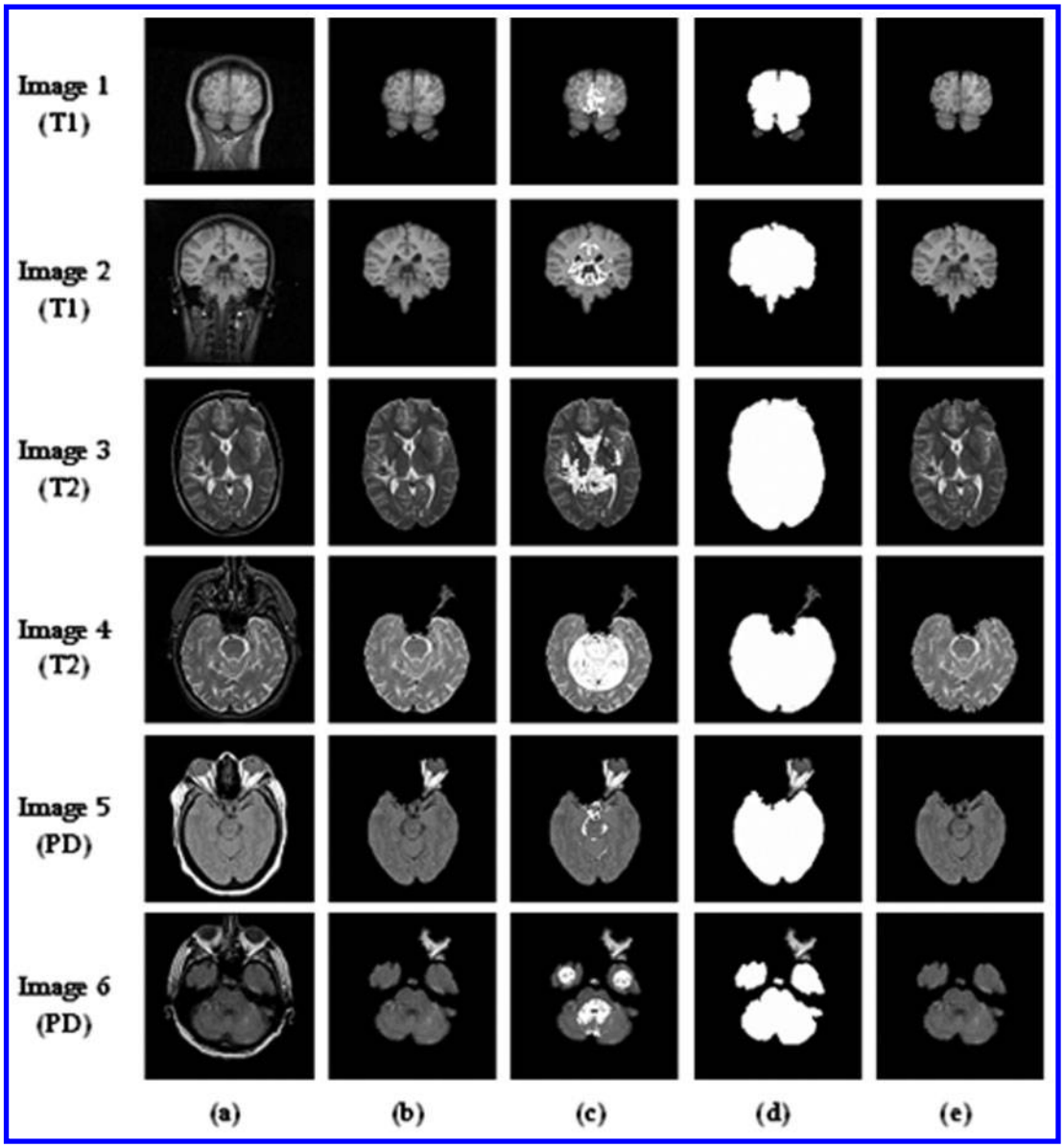

5 Seed points selection on T1-, T2- and PD-weighted images: *a* original image; *b* rough brain image; *c* selected seed points; *d* result of the proposed MRG segmentation; *e* segmented fine brain regions

Table 2 Parameters setting for the existing methods BET, BSE, WAT, HWA and GCUT and the proposed BSMRG method

Method	Fixed parameters	Value	Input image type
BET	Fractional intensity threshold	0·5	T1-, T2- and PD-weighted images
	Threshold gradient	0·0	
BSE	Diffusion iteration	3	T1-, T2- and PD-weighted images
	Diffusion constant	35	
	Edge constant	0·62	
	Erosion size	2	
WAT	Pre-flooding height	$H_{pf}=0{\cdot}11I_{max}+3{\cdot}5n$	T1-weighted images
HWA	Pre-flooding height	25% of I_{max}	T1-weighted images
	Post watershed threshold	$\sqrt[3]{\text{vol(basin)}}$	
	Curvature range	$r_{min}=3{\cdot}33$, $r_{max}=10$	
	Atlas-based force constants	$\lambda_D=0{\cdot}25$, $\lambda_C=0{\cdot}025$	
	Convergence threshold	0·5 mm	
GCUT	Intensity threshold for white mater	0·36	T1-weighted images
	Intensity control parameter	2·3	
BSMRG (proposed)	Overlapping ratio	90%	T1-, T2- and PD-weighted images
	SE for erosion	O_3	
	SE for dilation	O_3	
	Small hole size	25 pixels	
	Region growing threshold (t)	0·2	
	Neighbourhood for region growing	Four-connected neighbours	

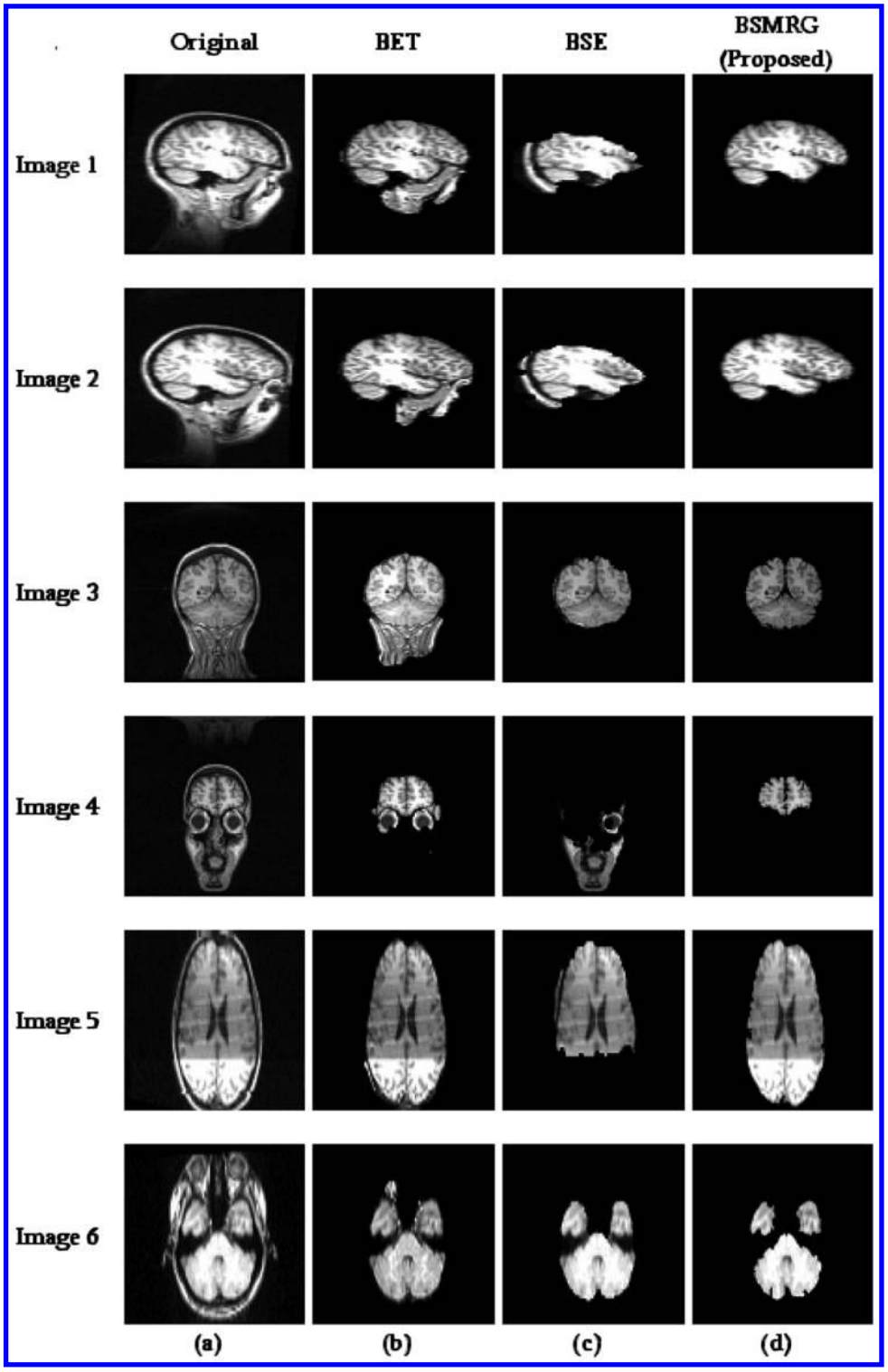

6 Brain regions extracted by the existing and proposed BSMRG methods for the selected sample slices from Dataset-1: *a* original T1-weighted images, extracted brain region by *b* BET, *c* BSE and *d* BSMRG methods

Dataset-1 to Dataset-4. The existing methods BET, WAT, HWA and GCUT were used with default parameter values. For BSE the default parameter values were changed as suggested by Hartley *et al.*[31] The summary of the various parameters and values assigned for these existing methods and the proposed method are given in Table 2.

The process of seed points selection on some of the randomly selected sample T1-, T2- and PD-weighted brain images of the selected datasets are depicted in Fig. 5. In this figure, Image 1 and Image 2 are T1-weighted images, T2-weighted images are given as Image 3 and Image 4 and PD-weighted images are shown as Image 5 and Image 6. Figure 5a is the original image and its corresponding rough brain image obtained by BSMRG method is shown in Fig. 5b in the same figure. The selected seed points after applying the seed points selection procedure are represented as white pixels as shown in Fig. 5c. The segmentation result for the images in Fig. 5c by using the proposed multi-seeded region growing method is given in Fig. 5d and the extracted fine brain regions are shown in Fig. 5e. The Image 4, Image 5 and

Table 3 Computed values of mean, *SD* and range for the parameters *D*, *J*, *FPR* and *FNR* by BET, BSE, WAT, HWA, GCUT and proposed BSMRG methods for Dataset-1

	D	*J*	*FPR*(%)	*FNR*(%)
Method	Mean (*SD*) [range]	Mean (*SD*) [range]	Mean (*SD*) [range]	Mean (*SD*) [range]
BET	0·74 (0·14)	0·61 (0·18)	79·9 (59·3)	0·1 (0·1)
	[0·53–0·90]	[0·36–0·81]	[22·7–179·4]	[0·0–0·4)
BSE	0·79 (0·21)	0·69 (0·22)	5·1 (3·1)	27·0 (24·1)
	[0–0·95]	[0–0·90]	[2·1–13·0]	[3·5–100]
WAT	0·76 (0·14)	0·64 (0·18)	18·4 (14·1)	24·5 (22·7)
	[0·47–0·92]	[0·31–0·86]	[5·2–61·2]	[0·1–62·7]
HWA	0·78 (0·21)	0·68 (0·21)	131·2 (308·2)	1·9 (6·5)
	[0·16–0·88]	[0·09–0·78]	[19·4–1060·2]	[0·0–28·9]
GCUT	0·85 (0·09)	0·75 (0·10)	38·3 (40·1)	**0·01** (0·02)
	[0·49–0·90]	[0·33–0·81]	[23·1–207·5]	[0·0–0·06]
BSMRG (proposed)	**0·971** (0·01)	**0·944** (0·02)	**0·55** (0·003)	2·94 (0·01)
	[0·94–0·98]	[0·89–0·96]	[0·1–0·82]	[0·51–8·33]
Computed values for the converted other orientations of Dataset-1 by the proposed BSMRG method				
Axial	0·978 (0·01)	0·958 (0·02)	65·25 (0·04)	2·66 (0·02)
	[0·959–0·991]	[0·921–0·986]	[58·24–66·67]	[2·35–10·91]
Sagittal	0·976 (0·01)	0·954 (0·02)	63·30 (0·04)	3·04 (0·02)
	[0·961–0·990]	[0·934–0·983]	[59·24–81·55]	[1·1–6·4]

Image 6 of Fig. 5b contains some additional non-brain tissues (eyes) in the rough brain image, though the proposed method separates it from the brain tissues. Hence, it is inferred from the results given in Fig. 5 that the proposed method efficiently identifies the seed points in all the selected images, irrespective of varying tissue contrast between T1-, T2- and PD-weighted images and thus, the devised seed points selection procedure is robust and perform well on all types of brain images.

After converting the coronal slices of Dataset-1 into sagittal and axial orientations, the performances of these converted volumes were tested by the BSMRG method. The segmentation result of selected sample images are shown in Fig. 6, in which Image 1 and Image 2 are T1-weighted sagittal images, Image 3 and Image 4 are coronal images and axial oriented images are given as Image 5 and Image 6. Figure 6b and c shows the segmented brain by the existing methods BET and BSE, respectively. The brain segmentation result of the BSMRG method is depicted in Fig. 6d. Compared to BET and BSE, the proposed method has accurately segmented the brain, whereas BET included additional non-brain tissues and BSE excluded the essential brain tissues and has also failed to find the brain in Image 4. Thus, the proposed multi-seeded region growing method exhibits better performance on all orientations of brain images compared to the conventional methods BET and BSE and has produced consistent results on Dataset-1.

For quantitative analysis, the Jaccard (J), Dice (D), false positive rate (FPR(%)) and false negative rate (FNR (%)) were calculated on the original and converted orientations of Dataset-1 and Dataset-2 by the equations (9) to (12) using the proposed BSMRG and the existing methods BET, BSE, WAT, HWA and GCUT methods.

The computed value of D, J, FPR(%) and FNR(%) for the Dataset-1 is given in Table 3. To compare the performance of the BSMRG method with the existing methods BET, BSE, WAT, HWA and GCUT using Dataset-1, the mean, standard deviation (SD) and range for the parameters D, J, FPR(%) and FNR(%) were also calculated and are given in Table 3. From Table 3, it is noted that, for the original coronal volume of Dataset-1, the best values of D=0·971 and J=0·944 were produced by BSMRG method. The best FPR(%) of 0·55 was recorded by BSMRG method. The D, J, FRP(%) and FNR(%) values were also computed for the converted axial and sagittal volumes of Dataset-1 and are given in the same table. It is evident from Table 3 is that the proposed method have exhibited consistence performance on all types of image orientation. Thus, it is also inferred that the proposed skull stripping method is

Table 4 Computed values of mean, *SD* and range for the parameters *D*, *J*, *FPR* and *FNR* by BET, BSE and proposed BSMRG methods for Dataset-2

	D	*J*	*FPR*(%)	*FNR*(%)
Method	Mean (*SD*) [range]	Mean (*SD*) [range]	Mean (*SD*) [range]	Mean (*SD*) [range]
BET	0·962 (0·01)	0·928 (0·02)	4·7 (0·001)	5·95 (0·02)
	[0·93–0·98]	[0·87–0·95]	[0·0005–0·0443]	[0·0200–0·1002]
BSE	**0·966** (0·01)	**0·937** (0·01)	**1·96** (0·001)	**1·12** (0·01)
	[0·77–0·99]	[0·64–0·99]	[0·0095–0·2078]	[0·0005–0·0387]
BSMRG (proposed)	0·951 (0·01)	0·908 (0·02)	2·19 (0·005)	1·96 (0·01)
	[0·894–0·969]	[0·809–0·940]	[1·56–3·63]	[0·15–6·28]
Computed values for the converted other orientations of Dataset-2 by the proposed BSMRG method				
Axial	0·973 (0·01)	0·948 (0·02)	41·59 (0·06)	1·55 (0·02)
	[0·948–0·985]	[0·901–0·971]	[30·95–49·16]	[0·12–8·1]
Sagittal	0·979 (0·007)	0·960 (0·01)	53·61 (0·03)	1·22 (0·01)
	[0·943–0·986]	[0·893–0·973]	[44·99–58·44]	[0·18–6·65]

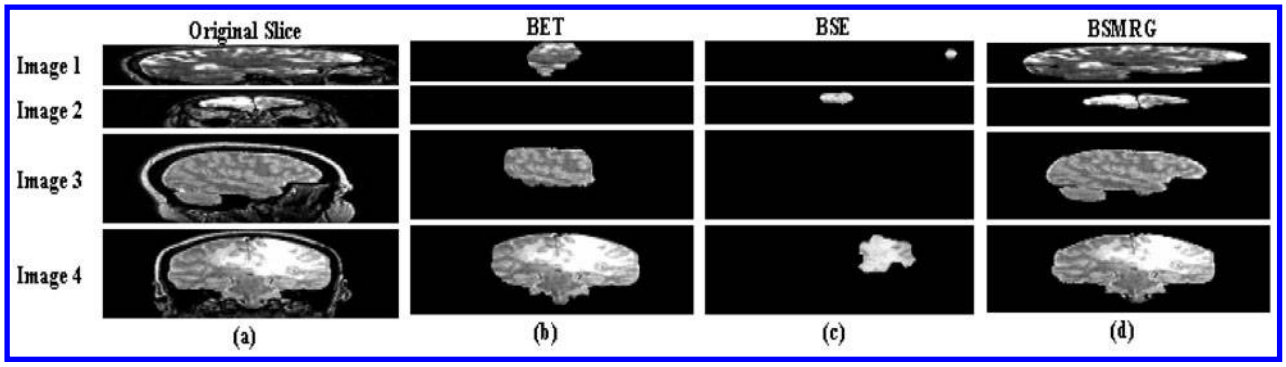

7 Brain segmentation result for T2- and PD-weighted images: *a* original image; segmented brain by *b* BET, *c* BSE and *d* proposed BSMRG methods

better at extracting the brain even if the brain images are affected with low/high image contrast, noises and various imaging artefacts.

The proposed BSMRG method was evaluated on Dataset-2 and the results are compared in terms of D, J, FPR(%) and FNR(%) values with the existing BET and BSE methods. The computed D, J, FPR(%) and FNR(%) values for BET, BSE and BSMRG methods on Dataset-2 for all the image orientations are given in Table 4. For Dataset-2, the existing method BET has produced stable performance on all the original volumes. Although BSE has produced best average D and J values, it has failed to extract the brain correctly in the volumes labelled 'S23' and 'S32' in Dataset-2. For these volumes, the proposed BSMRG method has obtained consistent and better skull stripping results. The BSMRG method have produced best values of D=0·979 and J=0·96 for the converted sagittal volumes of Dataset-2.

The qualitative performance of the proposed BSMRG method on T2- and PD-weighted images were evaluated using Dataset-3 and Dataset-4 (since repository of these volumes does not contain hand-stripped volumes) and has produced better result than the existing BET and BSE methods. The Dataset-3 and Dataset-4 originally contain axial oriented brain volumes. These volumes were converted into coronal and sagittal orientations. The performance of the proposed method was tested with these converted volumes and has produced better and consistence performance on all types of image orientations compared to the existing BET and BSE methods. A selected sample T2- and PD-weighted brain images of Dataset-3 and Dataset-4 along with the segmented brain obtained by the existing methods (BET and BSE) and the proposed BSMRG method are shown in Fig. 7. In Fig. 7, Image 1 and Image 2 are T2-weighted images and Image 3 and Image 4 are PD-weighted images. For these images the proposed method have produced good segmentation result (Fig. 7d), whereas the BET has failed to segment the brain in Image 2 and BSE in Image 3. The existing methods BET and BSE have not produced accurate segmentation result for other images in Fig. 7a.

Based on the comparative analysis, it is found that the conventional methods do not produce better results for T2- and PD-weighted images even after varying the values of their parameters as given in Table 5. In BET, the value of intensity threshold is varied from 0·1 to 0·9, and was found that, small values produce under-segmentation and large values produce over-segmentation. Therefore, BET

Table 5 Values of parameter varied and used for BET and BSE methods

Method	Parameter	Default value	Range of values varied	Value used
BET	Intensity threshold	0·5	0·1–0·9	0·5
	Threshold gradient	0·0	…	0·0
BSE	Diffusion iteration	3	1–10	3
	Diffusion constant	25	5–50	35
	Edge constant	0·64	0·50–0·75	0·62
	Erosion size	1	1–5	2

Table 6 The comparison of nature of datasets used and estimated processing time for BET, BSE and the proposed BSMRG methods

Method	Nature of the datasets used in the original work			Estimated processing time for the existing and the proposed methods for the datasets used in the proposed method (s/slice)
	Sample size	Slice thickness (mm)	Clinical	
BET	35 T1-weighted 6 T2-weighted 4 PD-weighted	0·8–6 mm	Normal subjects	<0·5
BSE	20 T1-weighted	3	Normal subjects	<0·5
BSMRG (proposed)	60 T1-weighted 20 T2-weighted 20 PD-weighted	1·5–5	Normal and pathological subjects	<5

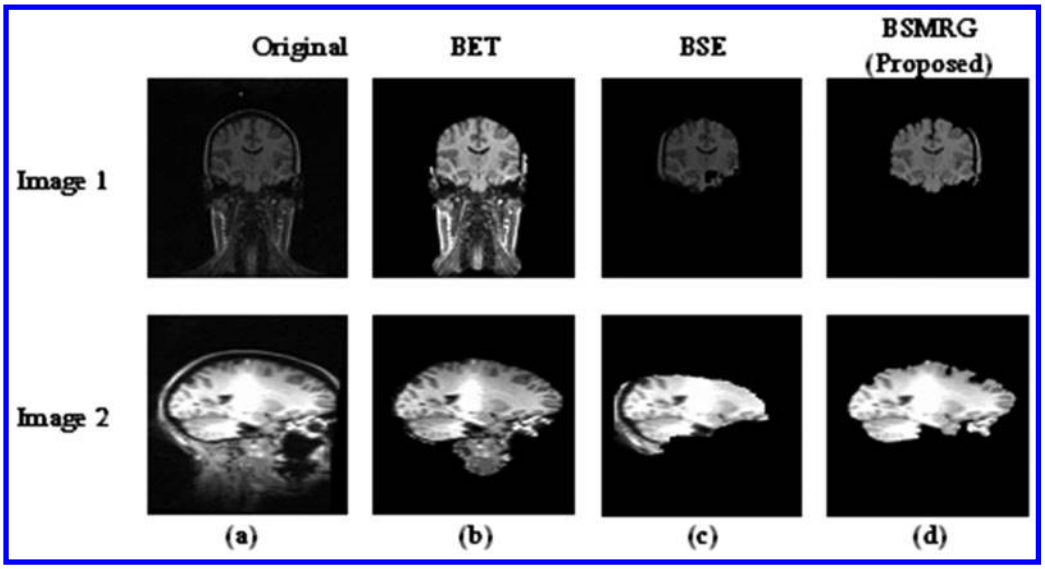

8 Illustration of over-segmentation and under-segmentation: *a* original image; extracted brain region by *b* BET, *c* BSE and *d* BSMRG methods

was used with default parameter values and for BSE, the parameter values were changed as Diffusion Iteration=3, Diffusion Constant=35, Edge Constant=0·62 and Erosion Size=2 as suggested by Hartley *et al.*[31]

From Tables 3 and 4 and Figs. 5, 6 and 7, it is observed that the proposed method performs well on all the three orientations of T1-, T2- and PD-weighted images, whereas the BET and BSE methods have not produced good results for T2- and PD-weighted images. The other existing methods WAT, HWA and GCUT compared in this paper are devised only for T1-weighted images as given in Table 2. The comparison of the nature of datasets used by the existing BET, BSE and the proposed BSMRG method, and the estimated time taken to extract the brain slice by these methods are given in Table 6.

Although the proposed method has exhibited the best performance on all types of image slices in Dataset-1 to Dataset-4, it has over-segmented/under-segmented the brain regions in some few slices as illustrated in Fig. 8. Because of the intensity homogeneity among the brain and non-brain regions, it is quite possible to group region satisfying the given region growing similarity criteria into brain region as shown in Image 1 of Fig. 8d. For a few other images, some brain pixels may appears too dark/bright because of the Intensity Non-Uniformity artefacts, which are ignored by the region growing criteria as depicted in Image 2 of Fig. 8. Similar results were also obtained by the conventional BET and BSE methods (Fig. 7b and c).

Conclusion

Brain segmentation in MRI human head scans using multi-seeded region growing BSMRG method developed in this article was tested with brain images of Dataset-1 to Dataset-4 containing 100 volumes of normal and abnormal T1-, T2- and PD-weighted images. The proposed automatic seed point selection procedure efficiently identifies the seed points based on the intensity profile of GM, WM and CSF of brain images. The brain are accurately segmented in all the orientations of T1-, T2- and PD-weighted images and have produced better results than the existing BET, BSE, WAT, HWA and GCUT methods. Thus, the BSMRG method is a suitable method to segment the brain from both normal and abnormal MR brain volumes of different types and orientations.

References

1. Haacke, E. M., Brown, R. W., Thompson, M. R. and Venkatesan, R. Magnetic Resonance Imaging: Physical Principles and Sequence Design, 1999 (John Wiley & Sons, New York).
2. Woods, R. P., Grafton, S. T., Watson, J. D. G., Sicotte, N. L. and Mazziotta, J. C. Automated image registration: II intersubject validation of linear and nonlinear models. *J. Comput. Assist. Tomogr.*, 1998, **22**, 153–165.
3. Lee, J. M., Yoon, U., Nam, S. M., Kim, J. H., Kim, I. Y. and Kim, S. I. Evaluation of automated and semi-automated skull-stripping algorithms using similarity index and segmentation error. *Comput. Biol. Med.*, 2003, **33**, 495–507.
4. Atkins, M. S., Siu, K., Law, B., Orchard, J. J. and Rosenbaum, W. L. Difficulties of T1 brain MRI segmentation techniques. *Proc. SPIE*, 2002, **4684**, 1837–1844.
5. Smith, S. M. Fast robust automated brain extraction. *Hum. Brain Mapp.*, 2002, **17**, 143–155.
6. Shattuck, D. W., Sandor-Leahy, S. R., Schaper, K. A., Rottenberg, D. A. and Leahy, R. M. Magnetic resonance image tissue classification using a partial volume model. *NeuroImage*, 2001, **13**, 856–876.
7. Hahn, K. K. and Peitgen, H. O. The skull stripping problem in MRI solved by single 3D watershed transform. *Lect. Notes Comput. Sci.*, 2000, **935**, 134–143.
8. Segonne, F., Dale, A. M., Busa, E., Glessner, M., Salat, D., Hahn, H. K. and Fischl, B. A hybrid approach to the skull stripping problem in MRI. *NeuroImage*, 2004, **22**, 1060–1075.
9. Sadananthan, A. S., Zheng, W., Chee, W. L. and Zagorodnov, V. Skull stripping using graph cuts. *NeuroImage*, 2010, **49**, 225–239.
10. Zhuang, A. H., Valentino, D. J. and Toga, A. W. Skull stripping magnetic resonance images using a model-based level sets. *NeuroImage*, 2006, **32**, 79–92.
11. Lao, Z., Shen, D. and Davatzikas, C. Statistical shape model for automatic skull stripping of brain images, Proc. 1st IEEE Int. Symp. on *Biomedical imaging: ISBI 2002*, Washington, DC, USA, June 2002, IEEE, pp. 855–858.
12. Park, G. J. and Lee, C. Skull stripping based on region growing for magnetic resonance images. *NeuroImage*, 2009, **47**, 1394–1407.
13. Carass, A., Cuzzocreo, J., Wheeler, M. B., Bazin, P. L., Resnick, S. M. and Prince, J. L. Simple paradigm for extra-cerebral tissue removal: algorithm and analysis. *NeuroImage*, 2011, **56**, 1982–1992.

14. Zhang, H., Liu, J., Zhu, Z. and Li, H. An automated and simple method for brain MR image extraction. *Biomed. Eng. Online*, 2011, **10**, 81.
15. Leung, K. K., Barnes, J., Modat, M., Ridgway, G. R., Bartlett, J. W., Fox, N. C. and Ourselin, S. Brain MAPS: an automated, accurate and robust brain extraction technique using a template library. *NeuroImage*, 2011, **55**, 1091–1108.
16. Hwang, J., Han, Y. and Park, H. Skull-stripping method for brain MRI using a 3D level set with a speedup operator. *J. Magn. Reson. Imaging*, 2011, **34**, 445–456.
17. Eskildsen, S. F., Coupe, P., Fonov, V., Manjón, J. V., Leung, K. K., Guizard, N., Wassef, S. N., Ostergaard, L. R. and Collins, D. L. BEaST: brain extraction based on non-local segmentation technique. *NeuroImage*, 2012, **59**, 2362–2373.
18. Galdames, F. J., Jaillet, F. and Perez, C. A. An accurate skull stripping method based on simplex meshes and histogram analysis in magnetic resonance images. *J. Neurosci. Methods*, 2012, **206**, 109–113.
19. Somasundram, K. and Kalavathi, P. Contour-based brain segmentation method for magnetic resonance imaging human head scans. *J. Comput. Assist. Tomogr*., 2013, **37**, 353–368.
20. Somasundram, K. and Kalavathi, P. Analysis of imaging artifacts in MR brain images. *Orient. J. Comput. Sci. Technol*., 2012, **5**, 135–141.
21. IBSR Dataset. Available at: <http://www.cma.mgh.harvard.edu/ibsr/index.html>, August 2012.
22. LPBA40 (LONI Probabilistic Brain Atlas). Available at: <http://www.loni.ucla.edu/Atlases/LPBA40/>, August 2012.
23. WBA (Whole Brain Atlas) MR brain image. Available at: <http://www.med.harvard.edu/AANLIB/home.html>, August 2012.
24. Somasundram, K. and Kalavathi, P. Medical image binarization using square wave representation. *Commun. Comput. Inf. Sci*., 2011, **140**, 151–158.
25. Somasundram, K. and Kalavathi, P. Medical image contrast enhancement based on gamma correction. *Int. J. Knowl. Manage. E-learn*., 2011, **3**, 15–18.
26. Gonzalez, R. C. and Woods, R. E. Digital Image Processing, 1992 (Addison-Wesley Publishing Company, Reading, MA).
27. Haralick, R. M. and Shapiro, L. G. Computer and Robot Vision — Volume I, 1992 (Addison-Wesley Publishing Company, Boston, MA).
28. Jain, A. K. and Dubes, R. C. Algorithms for Clustering Data, 1998 (Prentice Hall, Englewood Cliffs, NJ).
29. Jaccard, P. The distribution of flora in alpine zone. *New Phytol*., 1912, **11**, 37–50.
30. Dice, L. Measures of the amount of ecologic association between species. *Ecology*, 1945, **26**, 297–302.
31. Hartley, S. M., Scher, A. L., Kort, E. S. C., White, L. R. and Launer, L. J. Analysis and validation of automated skull stripping tools: a validation study based on 296 MR images from Honolulu Asia aging study. *NeuroImage*, 2006, **30**, 1179–1186.